Materials Today Physics 16 (2021) 100316

Contents lists available at ScienceDirect

Materials Today Physics

journal homepage: https://www.journals.elsevier.com/materials-today-physics

Epitaxial TiN/MgO multilayers with ultrathin TiN and MgO layers as hyperbolic metamaterials in visible region

J. Huang [a, *], Di Zhang [b], H. Wang [b, c, **]

[a] School of Materials, Sun Yat-sen University, Guangzhou, Guangdong 510275, China
[b] School of Materials Engineering, Purdue University, West Lafayette, IN 47907, USA
[c] School of Electrical and Computer Engineering, Purdue University, West Lafayette, IN 47907, USA

A R T I C L E I N F O

Article history:
Received 16 October 2020
Received in revised form
6 November 2020
Accepted 10 November 2020
Available online 13 November 2020

Keywords:
Multilayer
Hyperbolic metamaterial
Nitride
Epitaxial thin film
Optical anisotropy

A B S T R A C T

Multilayers with metal-dielectric stacks are considered as an effective approach to produce hyperbolic metamaterials (HMMs). However, fabricating ultrathin metal layers with high crystallinity for low-loss HMMs is very challenging. In this work, TiN has been applied as an alternative candidate to the noble metals, and TiN/MgO multilayers with varied numbers of layers and layer thicknesses have been designed. The microstructure study reveals that the thickness of TiN nanolayer is controlled as thin as 2.9 nm, 1.26 nm and 0.9 nm by varying the total number of layers, and the epitaxial quality of the multilayer films is high even with such ultrathin layers. Extraordinary optical properties have been achieved, such as plasmonic resonance in visible range, as well as strong optical anisotropy. In addition, the real part of dielectric permittivity (ε') shows opposite optical anisotropy in different wavelength ranges, i.e. $\varepsilon'_{\parallel}>0$, $\varepsilon'_{\perp}<0$ in the range of 350 nm–450 nm, and <0, $\varepsilon'_{\perp}>0$ under higher wavelength, which is a novel property realized in a multilayer system.

1. Introduction

Hyperbolic metamaterials (HMMs) possess remarkably anisotropic optical response, i.e., the permittivity presents opposite signs with different polarization directions [1–6]. A hyperbolic shape of isofrequency surface is a typical characteristic of HMMs, which results in high photonic density of states, as well as high k-mode propagation [7]. By engineering the light-matter interaction in nanoscale, HMMs are promising for a wide range of applications, such as subwavelength imaging [8–10], negative refraction [11–14], quantum emitters [15], quantum well (QW) light-emitting diodes (LEDs) [16], etc. Although there are some natural materials that show hyperbolic dispersion in defined wavelength range [17,18], most HMMs are artificially designed and fabricated. In general, two approaches have been employed to achieve artificial HMMs, i.e. metallic nanowire arrays [19–24], or metal/dielectric multilayers [16,25–31]. The morphology of metallic nanowires embedded in a dielectric matrix is usually achieved by electrochemical deposition of selected metals in a porous aluminum oxide template [20,21], or via co-deposition of metals and oxides using pulsed laser deposition (PLD) technique [19,22–24]. On the other hand, the metal/dielectric multilayers can be obtained by alternative growth of metal and dielectric materials [16,25–27]. In most cases of both approaches, a metal component is essential as an HMM subwavelength building block to provide the conducting electrons, which leads to the optical anisotropy.

Some of the major challenges to obtain HMM with good performance are the large negative permittivity and high optical losses, as well as processing challenges in synthesizing ultrathin metal layers or metal nanowires with high aspect ratio [32,33]. Nitrides and doped semiconducting oxides have been recently explored as potential alternatives to the noble metals, owing to their superior plasmonic properties in a particular wavelength range [33–36]. For example, TiN has been employed in the form of either nanowires [37] or multilayers [38,39] to achieve HMMs. TiN retains similar optical properties as Au [40], and could be epitaxially grown into ultrathin layer [41]. In addition, TiN is bio-compatible, CMOS-compatible, chemically inert, mechanically robust, and thermally stable with a high melting point exceeding 2700 °C, all made it a perfect alternative to Au for a wide range of applications [42].

* Corresponding author.
** Corresponding author. School of Materials Engineering, Purdue University, West Lafayette, IN 47907, USA.
E-mail addresses: huangjj83@mail.sysu.edu.cn (J. Huang), hwang00@purdue.edu (H. Wang).

https://doi.org/10.1016/j.mtphys.2020.100316
2542-5293/

In this work, multilayers of TiN/MgO with different numbers of layers and layer thickness have been designed and fabricated as tailorable HMM, as shown in the schematic illustrations, along with the low-mag scanning transmission electron microscopy (STEM) images and energy-dispersive X-ray spectra (EDS) chemical mappings, in Fig. 1. MgO is selected as the dielectric component, because of its nearly perfect lattice matching with TiN (a_{MgO} = 4.2112 Å, a_{TiN} = 4.241 Å), which allows the single-crystal-like epitaxial growth of the multilayers. Typically, the growth parameters for oxides and metals (or nitrides) are not compatible with each other. By careful selection of TiN and MgO, it is thus possible to deposit high epitaxial TiN/MgO multilayers with different layer thicknesses (thinnest layer thickness of 0.9 nm for TiN and 0.63 nm for MgO). This TiN/MgO multilayer design presents a new approach for HMMs with tailorable anisotropic properties, especially in the visible range.

2. Results and discussion

Three TiN/MgO multilayer films were fabricated, i.e. MT-5: $(TiN)_6(MgO)_5$ with 6 layers of TiN (t_{TiN} = 2.9 nm), and 5 layers of MgO (t_{MgO} = 1.29 nm), MT-10: $(TiN)_{11}(MgO)_{10}$ with 11 layers of TiN (t_{TiN} = 1.26 nm), and 10 layers of (t_{MgO} = 0.84 nm), and MT-20 $(TiN)_{21}(MgO)_{20}$ with 21 layers of TiN (t_{TiN} = 0.9 nm) and 20 layers of MgO (t_{MgO} = 0.63 nm). The thickness is thinner than the TiN/(Al,Sc)N superlattices fabricated by magnetron sputtering [39]. All the films were deposited on MgO (001) substrates. With such layer number and thickness, limited film quality degradation or inter-diffusion between adjacent layers takes place while strong anisotropy could be achieved in the multilayers. The θ-2θ X-ray diffraction (XRD) scans of the samples were first conducted and shown in Fig. S1, along with the reciprocal space maps (RSM) in Fig. S2. Satellite peaks are observed, resulting from the X-ray interference at the TiN:MgO interfaces, which also reveals the clean and sharp interfaces. Simultaneously, the satellite fringes presented in Fig. S2 further indicate the pesudomorphic growth (i.e., coherent growth between TiN/MgO layers) of the multilayers. The low-mag STEM images and EDS mappings of MT-5, MT-10 and MT-20 multilayers are shown in Fig. 1a, b and 1c, respectively, which further confirm the alternative growth of TiN and MgO with sharp heterointerfaces for all the samples.

To further explore the crystallinity of the films, MT-10 (as illustrated in Fig. 2a) has been selected for detailed microstructure characterizations. Fig. 2b exhibits a typical low-mag STEM image to show the entire thickness of the film, with corresponding geometric phase analysis (GPA) mapping (out-of-plane (ε_{yy}) strain) shown in Fig. 2c. Slightly compressive strain is generated in MgO layers, while slightly tensile strain is observed in TiN layers, both along out-of-plane direction. As the lattice constant of TiN (4.241 Å) is slightly larger than that of MgO (4.2112 Å), compressive TiN layer and stretched MgO layer along in-plane direction is expected, which denotes the opposite strain state in out-of-plane direction, as illustrated in the GPA mapping in Fig. 2c. A medium-mag STEM image with corresponding mask reversed fast Fourier transform (FFT) image are shown in Fig. 2d and e, respectively. Very high epitaxial quality of the multilayer is determined in Fig. 2d, and the

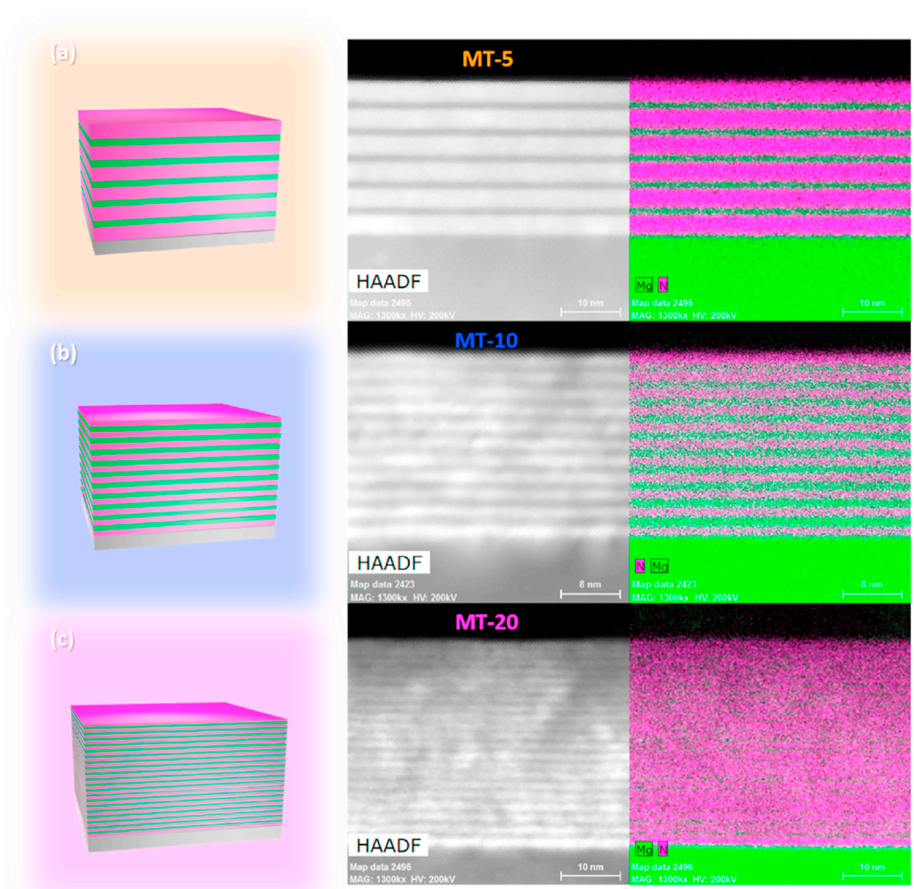

Fig. 1. Schematic illustrations, low-mag STEM images and corresponding EDS mappings of (a) MT-5, (c) MT-10, (e) MT-20 multilayer thin films.

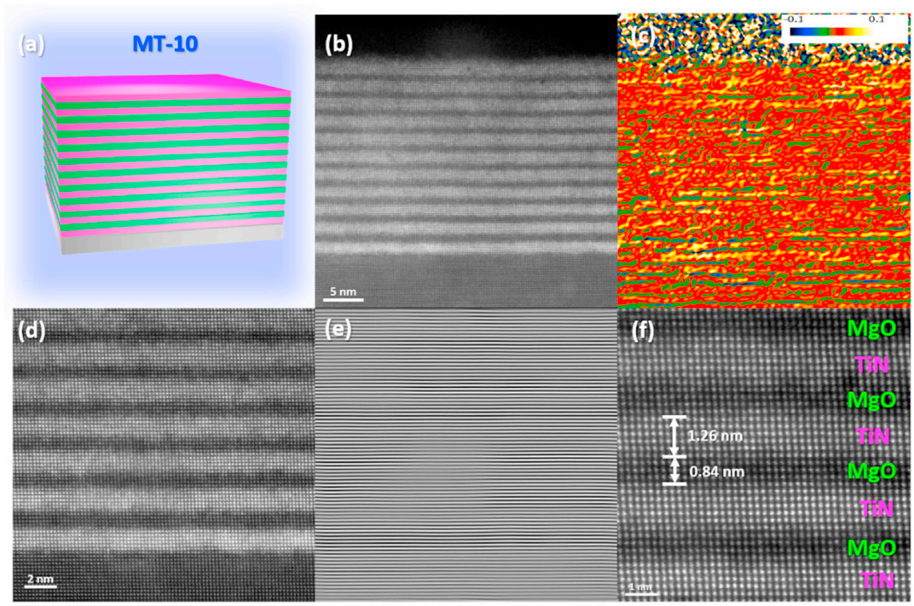

Fig. 2. Detailed microstructure of MT-10 multilayer thin film. (a) Schematic illustration; (b) STEM image to show the entire film with (c) geometric phase analysis (GPA) mapping; (d) a median-mag STEM image and (e) corresponding mask reversed FFT image; (f) a high-mag STEM image to show the film in atomic scale.

corresponding FFT image in Fig. 2e indicates the excellent crystallinity without visible defects existing in the film. We have further imaged the TiN:MgO interface area by high-resolution STEM, as shown in Fig. 2f. Relatively clear and abrupt interfaces are observed even in ultrathin layers, i.e. $t_{TiN} = 1.26$ nm, $t_{MgO} = 0.84$ nm. The ultrathin TiN layers with high quality could be ideal building blocks for HMM.

Next, the transmittance measurements of the multilayer films

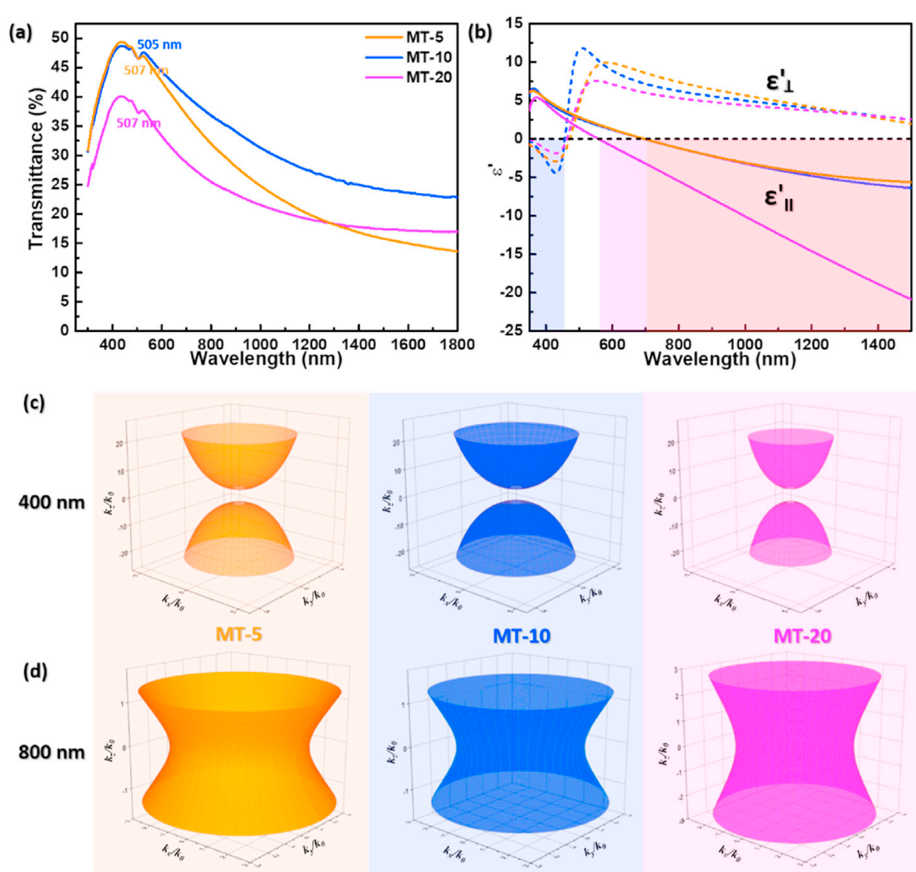

Fig. 3. (a) Transmittance spectral of all the three multilayers; (b) real part of complex dielectric function of all the multilayers in in-plane (parallel to the film surface) and out-of-plane (perpendicular to the film surface) directions; the extracted iso-frequency surfaces of the superlattice at (c) 400 nm and (d) 800 nm.

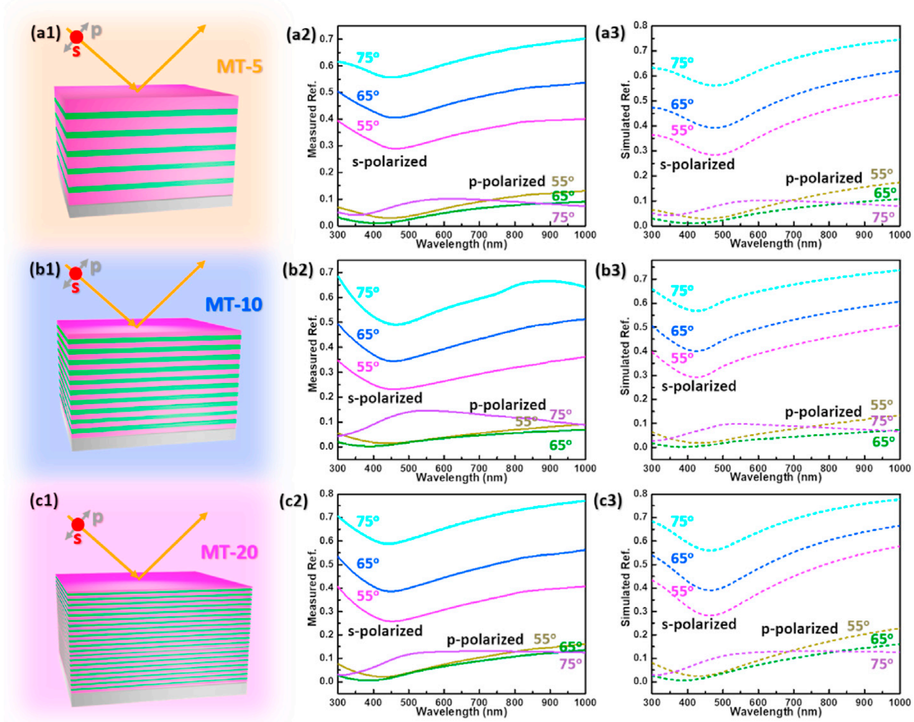

Fig. 4. Angle-dependent and polarization-resolved reflectivity of the multilayers. (a1), (b1), (c1) schematic illustrations to show the experimental setup; (a2), (b2), (c2) measured and (a3), (b3), (c3) simulated reflectivity spectral of MT-5, MT-10, MT-20 at different angles of incidence (55°, 65°, 75°) for p-polarized and s-polarized incident lights.

were conducted and the spectral of the three films is compared in Fig. 3a. Plasmonic feature at ~505 nm is observed for all the samples, which results from the plasmon resonance of the TiN nanolayer. Such plasmonic feature occurs at the wavelength comparable to the previous reported plasmonic TiN nanostructures [43–45]. The difference might come from the different shape, size and surrounding medium of the TiN nanostructures. Furthermore, angular-dependent ellipsometry measurements have been carried out to investigate the optical complex dielectric functions of the multilayer films, which were derived by fitting the measured ellipsometric constants phi (ϕ) plotted in Fig. S3. Because of the anisotropic nature of the TiN/MgO multilayers, a biaxial model has been applied, which refers to different dielectric permittivity in parallel ($\varepsilon_{\parallel}$) and perpendicular ($\varepsilon_{\perp}$) directions. Fig. 3b compares the real part of the dielectric permittivity ($\varepsilon'_{\parallel}$, $\varepsilon'_{\perp}$) of the three multilayer thin films. Interestingly, $\varepsilon'_{\parallel}$ and $\varepsilon'_{\perp}$ present opposite sings in two wavelength regions. In the wavelength of 350 nm–460 nm (region I), all the three multilayers possess $\varepsilon'_{\parallel}>0$ and $\varepsilon'_{\perp}<0$, which suggests transverse-positive dispersion and could be promising nanophotonic applications such as hyperlens [46]. In another side, transverse-negative ($\varepsilon'_{\parallel}<0$ and $\varepsilon'_{\perp}>0$) dispersion is obtained at higher wavelength (region II: 698 nm for MT-5, 696 nm for MT-10, 559 nm for MT-20), which demonstrates that MT-20 holds the strongest anisotropic property. Such wavelength regions cover more wavelength of light compared to the hyperbolic TiN/(Al,Sc)N superlattices [39], which indicates more potential applications of this TiN/MgO multilayers. The imaginary part (ε'') of dielectric permittivity for all the films are also plotted and compared in Fig. S4, pronounced feature at wavelength of ~500 nm is observed for all the samples, which is consistent with the above transmittance spectra. Moreover, optical iso-frequency k-space surface of the multilayers has been plotted at 400 nm (in region I) and 800 nm (in region II), which are exhibited in Fig. 3c and d, respectively. As seen, a hyperbola with two sheets and an open hyperboloid are observed at 400 nm and 800 nm, respectively, for all the multilayers, which demonstrates the different types of hyperbolic behaviors at different wavelength regions.

Lastly, angular dependent and polarization-resolved reflectivity was measured and the data was fitted for all the multilayers, with the incident angles of 55°, 65° and 75°, as shown in the schematic illustrations in Fig. 4a1-4c1. The measured (Fig. 4a2 for MT-5, Fig. 4b2 for MT-10, Fig. 4c2 for MT-20) and simulated (Fig. 4a3 for MT-5, Fig. 4b3 for MT-10, Fig. 4c3 for MT-20) reflectivity spectra present excellent matching. Basically, the reflectivity spectra of all the multilayers exhibit relatively similar trend with either s-polarized or p-polarized incident light, as the only difference for the samples is the layer number and thickness. Specifically, with s-polarized incident light, a pronounced feature at ~450 nm is determined, which corresponds to the plasmonic resonance of the TiN nanolayers. The results agree well with the above transmittance spectra and dielectric permittivity measurements, with minor differences. Furthermore, the reflectivity increases with increasing incident angle, which agrees with the classical electromagnetic theory. On the other hand, in the case of p-polarized incident light, the reflectivity is much lower and very different from that of s-polarized light, which further confirms the optical anisotropy of such multilayer HMM.

3. Conclusions

Epitaxial TiN/MgO multilayers with varied total numbers of layers and layer thicknesses have been deposited via PLD. Ultrathin layers of TiN and MgO were successfully achieved with excellent epitaxial quality, i.e. $t_{TiN} = 0.9$ nm, $t_{MgO} = 0.63$ nm. Such nitride-oxide multilayers exhibit interesting optical properties, including plasmonic resonance in the visible range, as well as optical anisotropic performance. More importantly, the multilayers present opposite signs of ε' in two wavelength ranges, which are transverse-positive ($\varepsilon'_{\parallel}>0$ and $\varepsilon'_{\perp}<0$) dispersion in the range of 350 nm–450 nm, and transverse-negative ($\varepsilon'_{\parallel}<0$ and $\varepsilon'_{\perp}>0$) dispersion under a higher wavelength region. The ultrathin TiN nanolayers in this TiN/MgO multilayers are considered as ideal building blocks for HMMs, which are promising for various photonic applications.

4. Experimental

The TiN/MgO multilayer thin films were deposited on MgO (001) substrates by alternative ablation of TiN and MgO targets, using pulsed laser deposition (PLD) method with a KrF excimer laser (Lambda Physik, $\lambda = 248$ nm). Before the deposition, the base pressure was pumped down to $<1 \times 10^{-6}$ Torr. During the deposition, the deposition temperature was kept at 700 °C with laser frequency of 5 Hz in vacuum condition for both TiN and MgO. After deposition, the chamber was naturally cooled down to room-temperature.

The crystal structure of the multilayer films was characterized by XRD (Panalytical X'Pert X-ray diffractometer). The STEM images with EDS mappings were taken by TEM (FEI Talos-F200X).

Transmittance measurement was done by UV–visible spectroscopy (Lambda 1050). During the measurement, a depolarized incident light was spotted in the direction perpendicular to the film surface. Angular-dependent ellipsometry measurements were carried out using a RC2 spectroscopic ellipsometer (J.A. Woollam Company). The optical dielectric permittivity of the multilayers was obtained by fitting the ellipsometry parameters psi (ϕ) using the VASE software. The fitting of the angle-dependent and polarization-resolved reflectivity was conducted by the same software, by setting s- or p-polarized light with incident angles of 55°, 65° and 75°.

Credit author statement

J.H. and H.W. conceived the idea. J.H. deposited the films and conducted XRD measurements. J.H. and D.Z. prepared the TEM samples and took the TEM images, as well as the optical measurements and fitting. All authors have contributed to the final draft of the paper.

Declaration of competing interest

The authors declare that they have no known competing financial interests or personal relationships that could have appeared to influence the work reported in this paper.

Acknowledgments

The work is supported by the U.S. National Science Foundation (DMR-1565822 for high resolution STEM imaging and DMR-2016453 for thin film growth). D.Z. and H.W. acknowledge the support from the U.S. Office of Naval Research under contract nos. N00014-20-1-2043 for the TEM effort. J.H. acknowledges the support from Guangdong Basic and Applied Basic Research Foundation (2019A1515111029).

Appendix A. Supplementary data

Supplementary data to this article can be found online at https://doi.org/10.1016/j.mtphys.2020.100316.

References

[1] A. Poddubny, I. Iorsh, P. Belov, Y. Kivshar, Hyperbolic metamaterials, Nat. Photon. 7 (2013) 948–957.
[2] L. Ferrari, C. Wu, D. Lepage, X. Zhang, Z. Liu, Hyperbolic metamaterials and their applications, Prog. Quant. Electron. 40 (2015) 1–40.
[3] D.R. Smith, D. Schurig, Electromagnetic wave propagation in media with indefinite permittivity and permeability tensors, Phys. Rev. Lett. 90 (2003): 077405.
[4] J. Zhang, H. Jiang, B. Gralak, S. Enoch, G. Tayeb, M. Lequime, Towards -1 effective index with one-dimensional metal-dielectric metamaterial: a quantitative analysis of the role of absorption losses, Optic Express 15 (2007) 7720–7729.
[5] M. Kim, S. So, K. Yao, Y. Liu, J. Rho, Deep sub-wavelength nanofocusing of UV-visible light by hyperbolic metamaterials, Sci. Rep. 6 (2016) 38645.
[6] S. So, J. Rho, Geometrically flat hyperlens designed by transformation optics, J. Phys. D Appl. Phys. 52 (2019) 194003.
[7] X. Yang, J. Yao, J. Rho, X. Yin, X. Zhang, Experimental realization of three-dimensional indefinite cavities at the nanoscale with anomalous scaling laws, Nat. Photon. 6 (2012) 450–454.
[8] Z. Liu, H. Lee, Y. Xiong, C. Sun, X. Zhang, Far-field optical hyperlens magnifying sub-diffraction-limited objects, Science 315 (2007) 1686.
[9] J. Rho, Z. Ye, Y. Xiong, X. Yin, Z. Liu, H. Choi, G. Bartal, X. Zhang, Spherical hyperlens for two-dimensional sub-diffractional imaging at visible frequencies, Nat. Commun. 1 (2010) 143.
[10] M. Byun, D. Lee, M. Kim, Y. Kim, K. Kim, J.G. Ok, J. Rho, H. Lee, Demonstration of nanoimprinted hyperlens array for high-throughput sub-diffraction imaging, Sci. Rep. 7 (2017) 46314.
[11] C. Argyropoulos, N.M. Estakhri, F. Monticone, A. Alu, Negative refraction, gain and nonlinear effects in hyperbolic metamaterials, Optic Express 21 (2013) 15037–15047.
[12] J. Valentine, S. Zhang, T. Zentgraf, E. Ulin-Avila, D.A. Genov, G. Bartal, X. Zhang, Three-dimensional optical metamaterial with a negative refractive index, Nature 455 (2008) 376–379.
[13] C. García-Meca, J. Hurtado, J. Martí, A. Martínez, W. Dickson, A.V. Zayats, Low-loss multilayered metamaterial exhibiting a negative index of refraction at visible wavelengths, Phys. Rev. Lett. 106 (2011): 067402.
[14] S. Bang, S. So, J. Rho, Realization of broadband negative refraction in visible range using vertically stacked hyperbolic metamaterials, Sci. Rep. 9 (2019) 14093.
[15] H.N. Krishnamoorthy, Z. Jacob, E. Narimanov, I. Kretzschmar, V.M. Menon, Topological transitions in metamaterials, Science 336 (2012) 205–209.
[16] D. Lu, H. Qian, K. Wang, H. Shen, F. Wei, Y. Jiang, E.E. Fullerton, P.K.L. Yu, Z. Liu, Nanostructuring multilayer hyperbolic metamaterials for ultrafast and bright green InGaN quantum wells, Adv. Mater. 30 (2018) 1706411.
[17] E.E. Narimanov, A.V. Kildishev, Naturally hyperbolic, Nat. Photon. 9 (2015) 214–216.
[18] J.D. Caldwell, A.V. Kretinin, Y. Chen, V. Giannini, M.M. Fogler, Y. Francescato, C.T. Ellis, J.G. Tischler, C.R. Woods, A.J. Giles, M. Hong, K. Watanabe, T. Taniguchi, S.A. Maier, K.S. Novoselov, Sub-diffractional volume-confined polaritons in the natural hyperbolic material hexagonal boron nitride, Nat. Commun. 5 (2014) 5221.
[19] L. Li, L. Sun, J.S. Gomez-Diaz, N.L. Hogan, P. Lu, F. Khatkhatay, W. Zhang, J. Jian, J. Huang, Q. Su, M. Fan, C. Jacob, J. Li, X. Zhang, Q. Jia, M. Sheldon, A. Alù, X. Li, H. Wang, Self-assembled epitaxial Au-oxide vertically aligned nanocomposites for nanoscale metamaterials, Nano Lett. 16 (2016) 3936–3943.
[20] J. Yao, Z. Liu, Y. Liu, Y. Wang, C. Sun, G. Bartal, A.M. Stacy, X. Zhang, Optical negative refraction in bulk metamaterials of nanowires, Science 321 (2008), 930-930.
[21] P.R. Evans, R. Kullock, W.R. Hendren, R. Atkinson, R.J. Pollard, L.M. Eng, Optical transmission properties and electric field distribution of interacting 2D silver nanorod arrays, Adv. Funct. Mater. 18 (2008) 1075–1079.
[22] J. Huang, X. Wang, X.L. Phuah, P. Lu, Z. Qi, H. Wang, Plasmonic Cu nanostructures in ZnO as hyperbolic metamaterial thin films, Mater. Today Nano 8 (2019) 100052.
[23] J. Huang, L. Li, P. Lu, Z. Qi, X. Sun, X. Zhang, H. Wang, Self-assembled Co-$BaZrO_3$ nanocomposite thin films with ultra-fine vertically aligned Co nanopillars, Nanoscale 9 (2017), 7970-7076.
[24] J. Huang, Z. Qi, L. Li, H. Wang, S. Xue, B. Zhang, X. Zhang, H. Wang, Self-assembled vertically aligned Ni nanopillars in CeO_2 with anisotropic magnetic and transport properties for energy applications, Nanoscale 10 (2018) 17182–17188.
[25] A.J. Hoffman, L. Alekseyev, S.S. Howard, K.J. Franz, D. Wasserman, V.A. Podolskiy, E.E. Narimanov, D.L. Sivco, C. Gmachl, Negative refraction in semiconductor metamaterials, Nat. Mater. 6 (2007) 946–950.
[26] T. Lee, J. Cho, D. Jeong, K. Lee, B. Park, T. Kim, Y. Kim, Y. Kim, Y. Nam, S. Kim, Pt/Alumina hyperbolic metafilms with high-temperature stability, wide wavelength tunability, and omnidirectional absorption, Phys. Status Solidi A 215 (2018) 1800287.
[27] H. Shen, D. Lu, B. VanSaders, J.J. Kan, H. Xu, E.E. Fullerton, Z. Liu, Anomalously weak scattering in metal-semiconductor multilayer hyperbolic metamaterials, Phys. Rev. X 5 (2015): 021021.
[28] X. Yang, J. Yao, J. Rho, X. Yin, X. Zhang, Experimental realization of three-dimensional indefinite cavities at the nanoscale with anomalous scaling

laws, Nat. Photon. 6 (2012) 450−454.
[29] G.V. Naik, J. Liu, A.V. Kildishev, V.M. Shalaev, A. Boltasseva, Demonstration of Al:ZnO as a plasmonic component for near-infrared metamaterials, Proc. Natl. Acad. Sci. U. S. A. 109 (2012) 8834−8838.
[30] M. Kim, D. Lee, T.H. Kim, Y. Yang, H.J. Park, J. Rho, Observation of enhanced optical spin hall effect in a vertical hyperbolic metamaterial, ACS Photonics 6 (2019) 2530−2536.
[31] H. Cho, S. So, T. Badloe, S. Bang, J. Rho, Critical layer thickness analysis of vertically stacked hyperbolic metamaterials for effective negative refraction generation, Adv. Theroy Simul. (2020) 2000138.
[32] O. Kidwai, S.V. Zhukovsky, J.E. Sipe, Effective-medium approach to planar multilayer hyperbolic metamaterials: strengths and limitations, Phys. Rev. A 85 (2012): 053842.
[33] G.V. Naik, V.M. Shalaev, A. Boltasseva, Alternative plasmonic materials: beyond gold and silver, Adv. Mater. 25 (2013) 3264−3294.
[34] J. Huang, X. Wang, N. Hogan, S. Wu, P. Lu, Z. Fan, Y. Dai, B. Zeng, R. Starko-Bowes, J. Jian, H. Wang, L. Li, R. Prasankumar, D. Yarotski, M. Sheldon, H. Chen, Z. Jacob, X. Zhang, H. Wang, Nanoscale artificial plasmonic lattice in self-assembled vertically aligned nitride-metal hybrid metamaterials, Adv. Sci. 5 (2018) 1800416.
[35] P. Guo, B.T. Diroll, W. Huang, L. Zeng, B. Wang, M.J. Bedzyk, A. Facchetti, T.J. Marks, R.P.H. Chang, R.D. Schaller, Low-loss near-infrared hyperbolic metamaterials with epitaxial ITOIn$_2$O$_3$ multilayers, ACS Photonics 5 (2018) 2000−2007.
[36] I. Yu, H. Cheng, C. Chang, Y. Lin, H. Chen, Y. Wang, Z. Yang, Substrate-insensitive atomic layer deposition of plasmonic titanium nitride films, Opt. Mater. Express 7 (3) (2017) 777−784.
[37] K. Yatsugi, K. Nishikawa, Highly anisotropic titanium nitride nanowire arrays for low-loss hyperbolic metamaterials fabricated via dynamic oblique deposition, Nanotechnology 30 (2019) 335705.
[38] J. Huang, X. Wang, D. Li, T. Jin, P. Lu, D. Zhang, P. Lin, H. Chen, J. Narayan, X. Zhang, H. Wang, 3D hybrid plasmonic framework with Au nanopillars embedded in nitride multilayers integrated on Si, Adv. Mater. Interfaces 7 (2020) 2000493.
[39] G.V. Naik, B. Saha, J. Liu, S.M. Saber, E.A. Stach, J.M.K. Irudayaraj, T.D. Sands, V.M. Shalaev, A. Boltasseva, Epitaxial superlattices with titanium nitride as a plasmonic component for optical hyperbolic metamaterials, Proc. Natl. Acad. Sci. U. S. A. 111 (2014) 7546.
[40] N.C. Chen, W.C. Lien, C.R. Liu, Y.L. Huang, Y.R. Lin, C. Chou, S.Y. Chang, C.W. Ho, Excitation of surface plasma wave at TiN/air interface in the Kretschmann geometry, J. Appl. Phys. 109 (2011): 043104.
[41] G.V. Naik, J.L. Schroeder, X. Ni, A.V. Kildishev, T.D. Sands, A. Boltasseva, Titanium nitride as a plasmonic material for visible and near infrared wavelengths, Opt. Mater. Express 2 (4) (2012) 478−489.
[42] U. Guler, G. Naik, A. Boltasseva, V. Shalaev, A. Kildishev, Performance analysis of nitride alternative plasmonic materials for localized surface plasmon applications, Appl. Phys. B 107 (2012) 285−291.
[43] W. Guo, R. Mishra, C. Cheng, B. Wu, L. Chen, M. Lin, S. Gwo, Titanium nitride epitaxial films as a plasmonic material platform: alternative to gold, ACS Photonics 6 (2019) 1848−1854.
[44] A.A. Hussain, B. Sharma, T. Barman, A.R. Pal, Self-powered broadband photodetector using plasmonic titanium nitride, ACS Appl. Mater. Interfaces 8 (2016) 4258−4265.
[45] C. Chang, J. Nogan, Z. Yang, W.J.M. Kort-Kamp, W. Ross, T.S. Luk, D.A.R. Dalvit, A.K. Azad, H. Chen, Highly plasmonic titanium nitride by room-temperature sputtering, Sci. Rep. 9 (2019) 15287.
[46] Z. Jacob, L.V. Alekseyev, E. Narimanov, Optical hyperlens: far-field imaging beyond the diffraction limit, Optic Express 14 (2006) 8247−8256.